Electronic Supplementary Material (ESI) for Journal of Materials Chemistry C.

Realizing ultrahigh recoverable energy density and superior charge-discharge performance in $NaNbO_3$-based lead-free ceramics via a local random field strategy

Junpeng Shi, Xiuli Chen*, Xu Li, Jie Sun, Congcong Sun, Feihong Pang, Huanfu Zhou

Collaborative Innovation Center for Exploration of Hidden Nonferrous Metal Deposits and Development of New Materials in Guangxi, Key Laboratory of Nonferrous Materials and New Processing Technology, Ministry of Education, School of Materials Science and Engineering, Guilin University of Technology, Guilin 541004, China.

* **Corresponding authors:**

E-mail addresses: cxlnwpu@163.com.

* Corresponding author. E-mail address: cxlnwpu@163.com

1. Experimental procedures

1.1 Fabrication of (1-*x*)$NaNbO_3$-*x*Bi($Mg_{2/3}Ta_{1/3}$)O_3 ceramics

(1-*x*)$NaNbO_3$-*x*Bi($Mg_{2/3}Ta_{1/3}$)O_3 (*x*BMT) ceramics were fabricated via the conventional solid-state reaction method. The raw materials are Na_2CO_3, Nb_2O_5, Bi_2O_3, MgO, and Ta_2O_5(≥99%). Stoichiometric proportions of the raw materials were mixed in alcohol by using zirconia balls for 6h. After drying, the mixed powders were calcined at 900 °C for 5h. The calcined powder was milled for 6h in the same way as the original powders. The resultant powders were mixed with 6wt% of polyvinyl alcohol (PVA) and pressed into pellets with 8mm in diameter and 1mm in thickness by uniaxial pressing at 200 MPa. The samples were coated with calcined powders of the same composition in order to minimize volatilization of alkaline elements and sintered at different temperatures, depending on the doping content, ranging from 1200 to 1330 °C for 2h in the air.

1.2 Characterization

The phase structures of the samples were analysed using an X-ray powder diffraction (XRD, Model X'Pert PRO; PA Nalytical, Almelo, Netherlands) with Cu K_α radiation (λ = 0.15406 nm). The microstructures of the samples were observed via a scanning electron microscopy (Model JSM6380-LV SEM, JEOL, Tokyo, Japan). The relative permittivity and loss tangent of the ceramics were measured using a precision impedance analyser (Model 4294A, Hewlett-Packard Co, Palo Alto, CA) in the

temperature range of -200°C to 300°C with the heating rate of 2°C/min. Polarization hysteresis loops were measured via a ferroelectric material parameters tester (RT66, Radiant Technologies, NM, USA). To better characterize the energy storage properties, the sintered samples were polished down to a thickness of 0.15 ± 0.01 mm and were coated via Ag electrode with a diameter of 2 mm. The dielectric breakdown strength (*BDS*) was measured at room temperature by using a voltage-withstand test device (RK2671AM). The energy release properties of ceramic capacitors were investigated via a charge-discharge platform with a specially-designed and high-speed capacitor discharge resistance, inductance, and capacitance load circuit (RLC).

2. Results and discussion

To provide further insights into the crystal structure and disorder characteristics of the *x*BMT ceramics, Raman spectroscopy was performed, and the results are shown in Fig. S1. Four main regions (v_1 is associated with the vibration of A-site cations, v_2 is related to the Nb^{5+} cation displacement and Nb-O vibrations (A_1), the v_3 and v_4 peaks mainly originate mainly from the NbO_6 octahedron stretching vibration, and the high-frequency region above v_5 is related to the A_1+E vibrations) are presented in Fig. S1, which are consistent with the previously reported perovskite structure [1-4]. The v_1 and v_2 peaks shift towards a lower wavenumber with an increase the BMT content, which indicates that the incorporation of BMT decreases the Nb^{5+} cation displacement and softens the bending vibration of Nb-O vibration. The v_2 peak gradually fades away with the increase in the BMT content, which may result from the higher symmetry. All the peaks become weaker in intensity and broader in shape with the increment of the BMT

content. This phenomenon may be related to the random distribution of Bi^{3+} and Na^{+} in A-sites due to their large differences in the radius and valence, as generally observed in doped $K_{0.5}Na_{0.5}NbO_3$ systems [5]. Moreover, the bands of the Nb-O vibrations and NbO_6 octahedra become broader with increasing *x*, which is a result of the B-site disorder in the *x*BMT ceramics by the $(Mg_{2/3}Ta_{1/3})^{3+}$ substitute for Nb^{5+} [6]. A typical dielectric relaxor behaviour is observed in the 0.22BMT ceramics, and a certain degree of cation disorder is indicated by the Raman studies [7]. These results further prove that the disorder of both A-site and B-site and structure complexity was enhanced, which had an important influence on the dielectric properties.

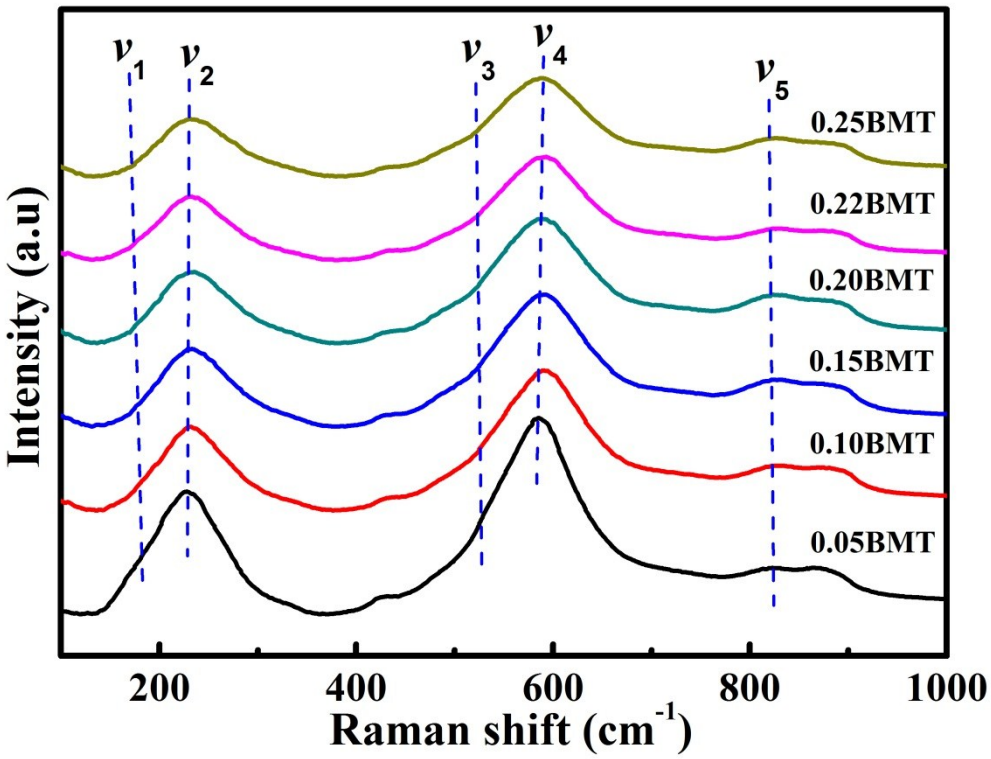

Fig. S1 Raman spectra of *x*BMT ceramics at room temperature.

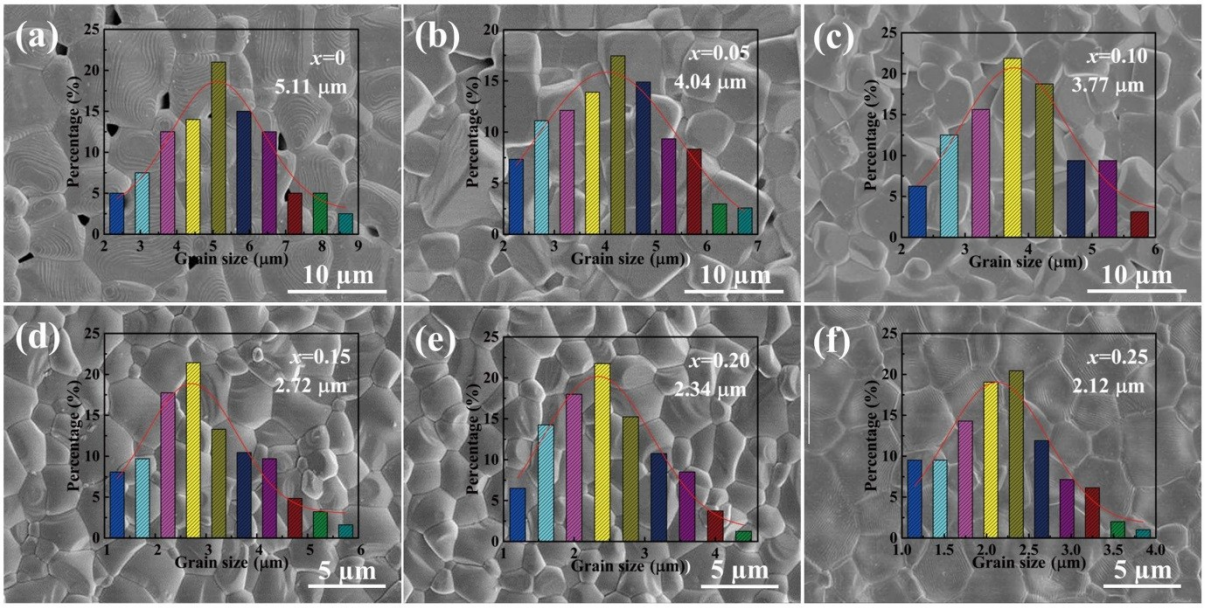

Fig. S2 SEM images of *x*BMT ceramics at optimum sintering temperature: (a) *x*=0, (b) *x*=0.05, (c) *x*=0.10, (d) *x*=0.15, (e) *x*=0.20 and (f) *x*=0.25. Insert show grain size distribution and average grain size of *x*BMT ceramics.

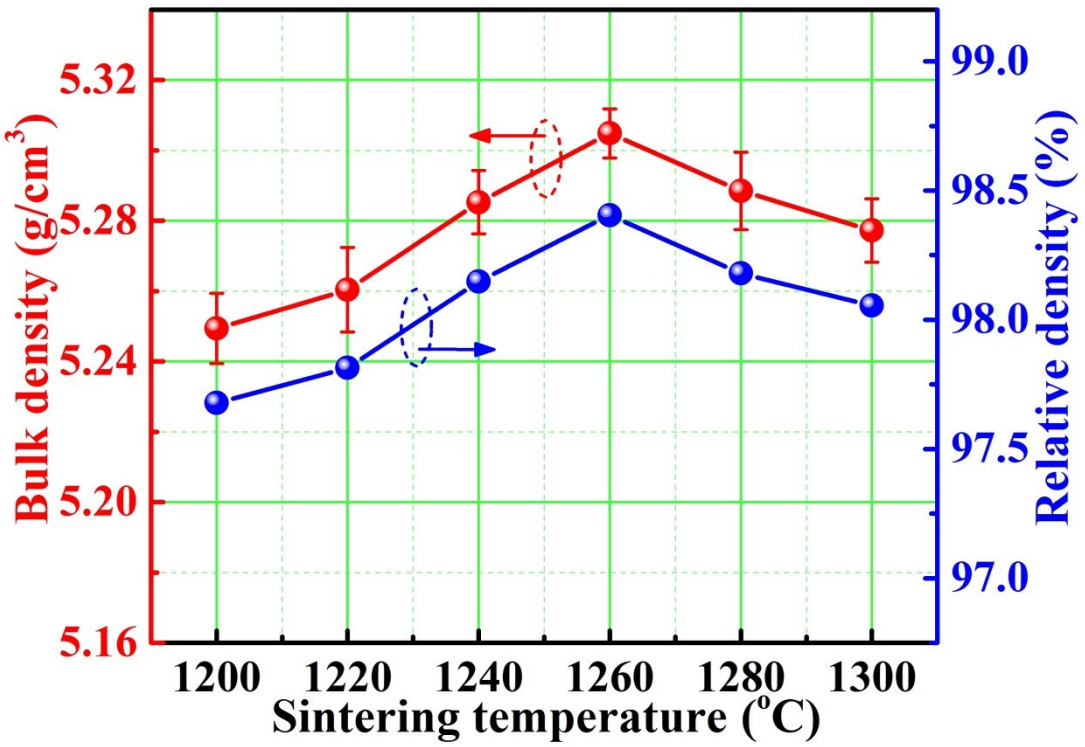

Fig. S3 Bulk and relative density of the 0.22BMT ceramics as functions of the sintering temperature.

The 0.22BMT ceramics demonstrate a thermally activated relaxation of dielectric loss at high temperature (>150 °C), characterized by the increase in tan δ with temperature (see Fig. 5a). The thermally activated relaxation is believed to be related to the movement of the dipoles formed by the associations of the defects involving oxygen vacancies formed under the reducing atmosphere during the sintering process. The presence of oxygen vacancies in the 0.22BMT ceramic was confirmed by XPS analysis (Fig. S4b). However, the presence of surface hydroxyl (−OH) and absorbed surface H_2O can be excluded due to the specimens being subjected to surface cleaning by Ar ion sputtering for 10 seconds before the XPS test [8]. Therefore, we can conclude that peak II mainly originates from the oxygen vacancies.

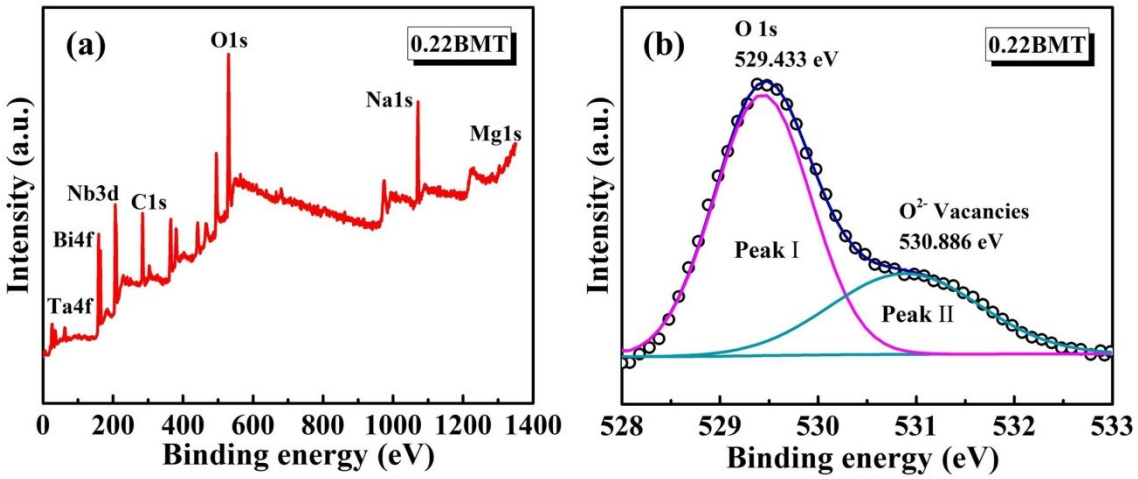

Fig. S4 Survey spectrum (a) and high resolution XPS of O 1s (b) for 0.22BMT ceramics sintered at their optimized temperatures.

Table S1. Comparison of the charge-discharge properties of the BMT ceramics and other reported ceramics.

Composition	E (kV/mm)	$t_{0.9}$ (ns)	C_D (A/cm^2)	P_D (MW/cm^3)	Ref.
$Pb_{0.90}La_{0.04}Ba_{0.04}(Zr_{0.616}Sn_{0.264}Ti_{0.12})O_3$	6.67	~1000	~242	~1.95	[9]
$Pb_{0.925}La_{0.05}(Zr_{0.42}Sn_{0.40}Ti_{0.18})O_3$	3.5	~65	~183	~3.2	[10]
$Pb_{0.93}La_{0.04}Nb_{0.02}(Zr_{0.42}Sn_{0.40}Ti_{0.18})_{0.98}O_3$	4.0	~500	~143	~2.9	[11]
$Pb_{0.87}Ba_{0.1}La_{0.2}(Zr_{0.6}Ti_{0.07}Sn_{0.33})O_3$	6.0	/	~223	~6.69	[12]
BNT-BT-0.32SBT	6.0	~675	~400	~12.0	[12]
$Na_{0.7}Bi_{0.1}NbO_3$	10.0	~155	~1250	~62.5	[13]
$0.91NaNbO_3$-$0.09Bi(Zn_{0.5}Ti_{0.5})O_3$	11.0	~250	~275	~20	[14]
$0.78NaNbO_3$-$0.22Bi(Mg_{2/3}Ta_{1/3})O_3$	14.0	~23	~538	~38	This work

.

References

[1] Y. P. Pu, M. T. Yao, H. R. Liu and T. Fromling, *J. Eur. Ceram. Soc*., 2016, **36**, 2461-2468.

[2] S. N. Tripathy, K. K. Mishra, S. Sen and D. K. Pradhan, *J. Am. Ceram. Soc*., 2014, **97**, 1846-1854.

[3] Q. Li, J. Wang, Y. Ma, L. T. Ma, G. Z. Dong and H. Q. Fan, *J. Alloys. Compd*., 2016, **663**, 701-707.

[4] B. Parija, S. K. Rout, L. S. Cavalcante, A. Z. Simoes, S. Panigrahi, E. Longo and N. C. Batista, *Appl. Phys. A*., 2012, **109**, 715-723.

[5] Q. Liu, Y. C. Zhang, L. Zhao, J. Gao, Z. Zhou, K. Wang, X. W. Zhang, L. T. Li and J. F. Li, *J. Mater. Chem. C*, 2018, **6**, 10618-10627.

[6] L. Zhang, Y. Pu and M. Chen, *J. Alloys Compd*., 2019, **775**, 342-347.

[7] B. Zalar, V. V. Laguta and R. Blinc, *Phys. Rev. Lett*., 2003, **90**, 037601.

[8] Z. Hou, O. Yokota, T. Tanaka and T. Yashima, *Appl. Catal. A*., 2003, **253**, 381-387.

[9] R. Xu, Z. Xu, Y. Feng, H. He, J. Tian and D. Huang, *J. Am. Ceram. Soc*., 2016, **99**, 2984.

[10] H. Zhang, X. Chen, F. Cao, G. Wang, X. Dong, Z. Hu and T. Du, *J. Am. Ceram. Soc.,* 2010, **93**, 4015.

[11] X. Chen, H. Zhang, F. Cao, G. Wang, X. Dong, Y. Gu, H. He and Y. Liu, *J. Appl. Phys.,* 2009, **106**, 034105.

[12] F. Li, K. Yang, X. Liu, J. Zou, J. Zhai, B. Shen, P. Li, J. Shen, B. Liu and P. Chen, *Scripta. Mater.,* 2017, **141**, 15.

[13] M. Zhou, R. Liang, Z. Zhou and X. Dong, *J. Mater. Chem. A*, 2018, **6**, 17896.

[14] Y. Fan, Z. Zhou, R. Liang and X. Dong, *J. Eur. Ceram. Soc*., 2019, **39**, 4770-4777.